Journal of Building Engineering 7 (2016) 239–245

Contents lists available at ScienceDirect

Journal of Building Engineering

journal homepage: www.elsevier.com/locate/jobe

Dynamic model for measurement of convective heat transfer coefficient at external building surfaces

K.E. Anders Ohlsson *, Ronny Östin, Staffan Grundberg, Thomas Olofsson

Department of Applied Physics and Electronics, Umeå University, SE-90187 Umeå, Sweden

ARTICLE INFO

Article history:
Received 7 April 2016
Received in revised form
31 May 2016
Accepted 7 June 2016
Available online 8 June 2016

Keywords:
Convective heat transfer coefficient
Heat balance
Measurement uncertainty
Thermal network modelling
Dynamic sensor model

ABSTRACT

Uncertainties in current empirical models for the convective heat transfer coefficient (CHTC) have large impact on the accuracy of building energy simulations (BES). These models are often based on measurements of the CHTC, using a heated gradient sensor, where steady-state convective air flow is assumed. If this requirement is not fulfilled there will be a dynamic measurement error. The objectives were to construct a validated dynamic model for the heated gradient sensor, and to use this model to improve accuracy by suggesting changes in sensor design and operating procedure. The linear thermal network model included three state-space variables, selected as the temperatures of the three layers of the heated gradient sensor. Predictions of the major time constant and temperature time evolution were in acceptable agreement with experimental results obtained from step-response experiments. Model simulations and experiments showed that the sensor time constant increases with decreasing CHTC value, which means that the sensor response time is at maximum under free convection conditions. Under free convection, the surface heat transfer resistance is at maximum, which cause enhanced heat loss through the sensor insulation layer. Guidelines are given for selection of sampling frequency, and for evaluation of dynamic measurement errors.

1. Introduction

The convective heat flux q_c (W m^{-2}) from the building aboveground external surface is an important heat transfer process in the simulation of building energy performance. Usually, q_c is expressed as:

$$q_c = h_c(T_s - T_a) \quad (1)$$

where h_c (W m^{-2} K^{-1}) is the CHTC, T_s (K) is the building exterior surface temperature, and T_a (K) is the outdoor air temperature. The h_c coefficient depends on several factors, for examples building geometry, surface roughness, air flow pattern, and wind speed V (ms^{-1}) at some reference position. Many empirical models exist that correlate h_c and V in specific cases, some based on wind tunnel studies of flat plates (see e.g. Jürges [1]), while other models stem from field h_c measurements, using a sensor placed on the building surface [2–6]. There is a high uncertainty in the h_c values predicted by such empirical correlations, and when these values are used as input data to BES programs, this leads to uncertainty in the simulation results [7,8]. Part of the uncertainty in predicted h_c values from empirical models is due to measurement error in h_c.

There exists several methods for measurement of the heat flux and external CHTC (see reviews by [9–11]). Among these methods, the most commonly used within the field of building physics for measurement of CHTC is the heated gradient sensor type, as pioneered by Ito et al. [2]. The heated gradient sensor consists of a gradient heat flux meter (HFM), heated from its back side, using a resistive heater, and equipped with a thermometer for measurement of its front surface temperature T_s (K). The HFM estimates the conductive heat flux q_d (W m^{-2}) through the sensor by measuring the temperature gradient across a slab, using a series of thermocouples. The sensor front surface is in contact with the air boundary layer, whose h_c value is to be measured. The momentary heat balance of the sensor front surface is given by:

$$q_d + I_s/a = q_r + q_c \quad (2)$$

where a is the sensor surface area, I_s (W) is the short-wave solar radiation, and q_r (W m^{-2}) is the net thermal radiation:

$$q_r = \varepsilon_s \sigma \left(T_s^4 - T_r^4\right) \quad (3)$$

with ε_s = the surface emissivity, σ = the Stefan-Boltzmann constant (5.67×10^{-8} W m^{-2} K^{-4}), and T_r (K) = the mean radiant

* Corresponding author.
E-mail address: anders.ohlsson@umu.se (K.E.A. Ohlsson).

http://dx.doi.org/10.1016/j.jobe.2016.06.005
2352-7102/

temperature. The heat balance of Eq. (2) has been used in various ways for estimation of h_c. In the Ito method [2], for example, two sensors were used simultaneously, which enabled the effects from I_s and q_r to be cancelled out. If a single sensor was used (e.g. [4–6]) then I_s and q_r are first estimated separately, and then h_c is obtained by rearranging Eqs. (1) and (2) into:

$$h_c=\frac{q_c}{T_s-T_a}=\frac{q_d+I_s/a-q_r}{T_s-T_a} \tag{4}$$

Because the heat balance of Eq. (2) does not include heat storage in the sensor body, its application for determination of h_c, by Eq. (4), is valid only when there is no change in stored heat, i.e. when the input quantities of Eq. (4) are at steady-state. Studies where heat storage is taken into account in the heat balance of the heated gradient sensor are rare, and we know only one such work, that of Jayamaha et al. [5], although their sensor was operated with a control system set to keep the rate of heat storage equal to zero. To ensure that steady-state conditions prevail during the measurement of h_c, the sensor response time should be shorter than the time-scale of variations in the environmental parameters involved, e.g. in T_a, T_r, I_s, and in wind speed V.

The objective of the present work was to construct and validate a dynamic model of the heated gradient sensor [2] for measurement of the local CHTC at exterior building surfaces. This model enabled evaluation of effects on measurement accuracy due to limited sensor response time. It also yielded suggestions for improvement of the sensor design, and for selection of sensor operating conditions.

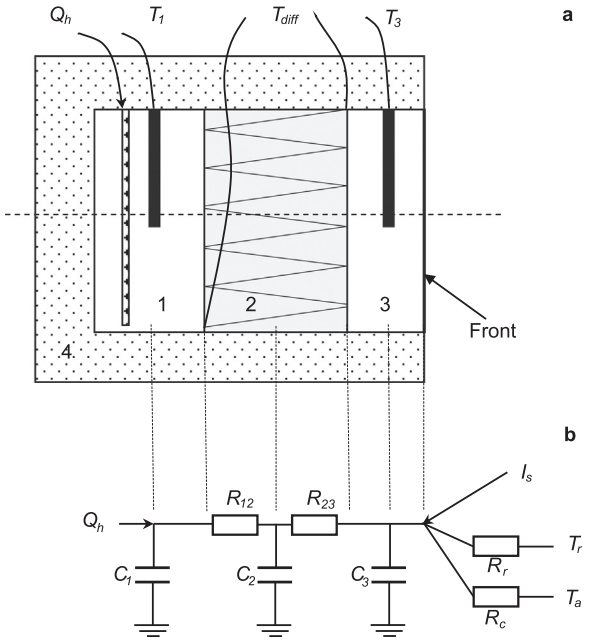

Fig. 1. (a) Schematic cross-sectional drawing of the CHTC sensor, with cylindrical symmetry around the center axis (dashed line). The bottom (1), HFM (2), and top (3) layers, were surrounded by insulation (4), except at the sensor front surface. The electrical heater supplied the heat flux Q_h. The temperatures T_1 and T_3 were measured using PRT probes inserted into the bottom and top layers, respectively. The HFM series of thermocouples measured the temperature difference T_{diff} across the HFM layer. (b) The thermal RC network model.

2. Thermal RC network model

Among the approaches to modelling of thermal dynamic systems, thermal network models are particularly useful, since they incorporate the system behavior into a limited number of state variables, the system temperatures or heat fluxes X_i (K). The time evolution of the system could then be expressed by the time derivative of the vector $\boldsymbol{X}(t)$ as:

$$\dot{\boldsymbol{X}}=f\left(\boldsymbol{X}(t),\boldsymbol{W}(t)\right) \tag{5}$$

where f is a (non-linear) function of the momentary values of $\boldsymbol{X}(t)$ and $\boldsymbol{W}(t)$, and $\boldsymbol{W}(t)$ is the vector of input variables (here, the electrically supplied heat flux, and the environmental parameters). The pseudo-bond graph method (ref. [12], ch.12) was here applied to describe the h_c sensor as a thermal network consisting of resistive (R) and capacitive (C) components, in analogy to electrical RC networks.

Essentially, the h_c sensor, as used by [2–6], consists of a stack of three layers (cf. Fig. 1(a)): (1) the metal bottom layer, which evenly distributes the heat flux Q_h (W), supplied by an electrical heater, over the sensor cross-sectional area a (m^2), (2) the HFM layer, and (3) the metal top layer, which at its front surface emits heats by radiation and convection. Fig. 1(b) shows the thermal RC network, where the bottom and top layers were modelled as pure capacitances, C_1 and C_3 ($J\,K^{-1}$), respectively, since their resistances were negligibly small in comparison to the other thermal resistances of the sensor (cf. Table 1). However, the HFM layer, with its thermal resistance R_2 (KW^{-1}), was modelled using three elements: one center capacitance C_2, and two flanking resistances, R_{12} and R_{23} ($R_2 = R_{12} + R_{23}$). The front surface was thermally connected to its surrounding through radiative and convective thermal resistances, R_r and R_c (KW^{-1}), respectively. The back-side of the sensor, and its side surfaces, faced an insulation layer, which is modelled here as an adiabatic wall, i.e. having an infinite thermal resistance (does not appear in the RC network).

The R and C quantities were estimated from layer thickness H (m), layer thermal conductivity λ ($W\,m^{-1}\,K^{-1}$), density ρ ($kg\,m^{-3}$), and specific heat capacity c_v ($J\,kg^{-1}\,K^{-1}$), as follows:

$$R=\frac{H}{\lambda a} \tag{6}$$

$$C=\rho a H c_v \tag{7}$$

With a sensor radius $r = 40$ mm, we get $a = 5.0\cdot 10^{-3}\,m^2$. The specification of the HFM (model HFP01, Hukseflux Thermal Sensors, Delft, Netherlands) states that $\lambda_{HFM} = 0.8\,W\,m^{-1}\,K^{-1}$, $H = 0.005$ m, and that its response time is $\pm$ 3 min. Assuming that this response time equals the thermal time constant, we obtained the HFM layer time constant as $\tau_{HFM}=180s = R_2C_2$. With $R_2 = 1.25\,KW^{-1}$, estimated based on Eq. (6), we then estimated C_2 to equal $144\,J\,K^{-1}$. We also obtain $\rho c_v=C_2/(aH)=5.76\cdot 10^6\,J\,K^{-1}\,m^{-3}$. Table 1 summarizes the parameter estimates of the sensor thermal network model.

The convective heat flux Q_c (W) at the sensor top surface was given as:

$$Q_c=q_c a=\frac{1}{R_c}\left(T_s-T_a\right) \tag{8}$$

where R_c (KW^{-1}) is the convective heat transfer resistance. By comparison with Eq. (1), we obtained $R_c=1/h_c a$. For the long-wave radiative heat flux Q_r (W) we have:

$$Q_r=q_r a=\varepsilon_s \sigma a\left(T_s^4-T_r^4\right) \tag{9}$$

Due to moderate temperature differences (T_s-T_r), Eq. (9) was here linearized into:

$$Q_r=\frac{1}{R_r}\left(T_s-T_r\right) \tag{10}$$

Table 1
Thermophysical properties of the sensor L system components.

	Model RC element	λ W m^{-1}K^{-1}	ρ kg m^{-3}	c_v J kg^{-1}K^{-1}	H m	R KW^{-1}	C JK^{-1}
Bottom[a]	C_1	401	8933	385	0.024	0.012	415
Top[a]	C_3				0.012	0.006	207
HFM[b]	$R_{12} = R_{23}$	0.80	–	–	0.0025	0.625	–
HFM[b]	C_2	–	ρc_v=5.76•10^6		0.005	–	144
Insulation[c]	–	0.035	55	1210	0.060	155	18
Radiation[d]	R_r	–	–	–	–	36.1	–
Convection[e]	R_c	–	–	–	–	5.0	–

[a] Copper, with materials data at 300 K obtained from ref. [13].
[b] Data from HFM specification.
[c] The insulation layer was not included into the model. Table A3, ref. [13], provided ρ and c_v data for "extruded polystyrene". Only the bottom layer surface circular and peripheral areas are included in the estimate of R and C.
[d] T_{sr}=295K, and $\varepsilon_s = 0.943$.
[e] Assuming that $h_c = 40$ W m^{-2} K^{-1}.

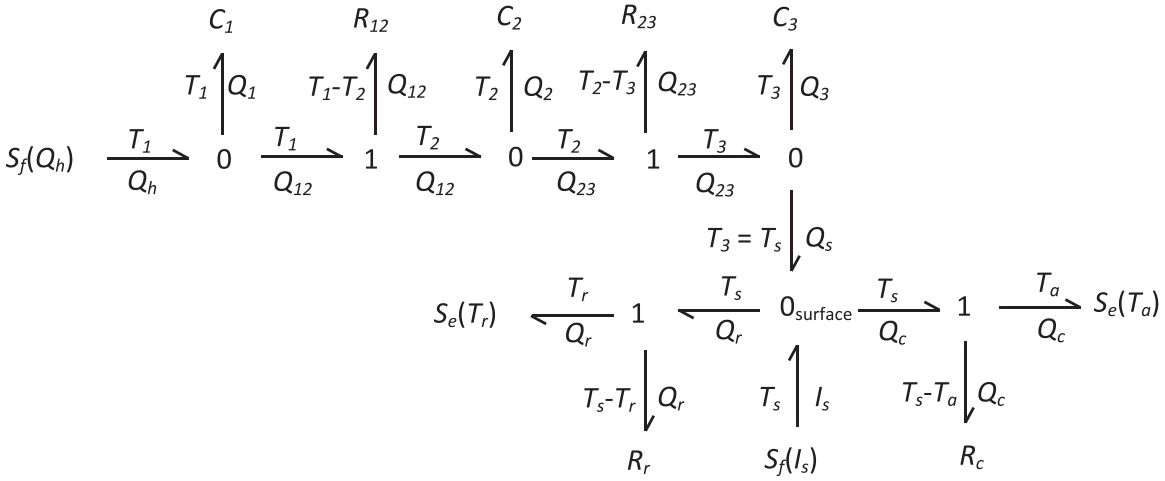

Fig. 2. Pseudo bond graph of the CHTC sensor. S_f is source of heat flux, and S_e is source of temperature. At parallel junctions (0), the temperature is equal for all bonds, while at series junctions (1), the heat flux is equal for all bonds. The half-arrows signify the direction of heat flux.

where R_r=$1/\left(4\varepsilon_s\sigma a\bar{T}_{sr}^3\right)$, and $\bar{T}_{sr}$=$(T_s+T_r)/2$ (see ref. [14]).

Fig. 2 shows the pseudo bond graph of the CHTC sensor, which provide a systematic way to describe the heat flux through the system, and how the heat flux and temperature quantities are related within the system. The rate of heat storage into the k:th C element is given as: Q_k=Q_{in}−Q_{out}, i.e. the difference between ingoing and outgoing heat fluxes. The heat flux through the resistance R_{ij} is driven by the difference in entrance and exit temperatures, T_i−T_j, and equals: Q_{ij}=$(T_i-T_j)/R_{ij}$. The conductive heat flux Q_s reaching the sensor top surface is expressed as Q_s= − I_s+Q_r+Q_c, which is the condition met at the surface parallel junction (0_{surface}; see Fig. 2), and corresponds to Eq. (2), the heat balance at the sensor top surface. With the temperature T_k of the capacitance element C_k selected as a state variable (here we have three sensor layers, corresponding to three state variables), we obtain the k:th state equation (cf. Eq. (5)) as:

$$\dot{X}_k=\dot{T}_k(t)=\frac{Q_k(t)}{C_k} \tag{11}$$

where Q_k could be expressed as a linear function of the state variables T_i, and the input variables Q_h, I_s, T_r and T_a. With T_3=T_s, the state equations in matrix form are as follows:

$$\dot{\boldsymbol{T}}=\boldsymbol{AT}+\boldsymbol{B}Q_h+\boldsymbol{EU}=$$
$$\begin{bmatrix} -\frac{1}{C_1R_{12}} & \frac{1}{C_1R_{12}} & 0 \\ \frac{1}{C_2R_{12}} & -\frac{1}{C_2}\left(\frac{1}{R_{12}}+\frac{1}{R_{23}}\right) & \frac{1}{C_2R_{23}} \\ 0 & \frac{1}{C_3R_{23}} & -\frac{1}{C_3}\left(\frac{1}{R_{23}}+\frac{1}{R_r}+\frac{1}{R_c}\right) \end{bmatrix} \bullet \begin{bmatrix} T_1 \\ T_2 \\ T_3 \end{bmatrix} + \begin{bmatrix} \frac{1}{C_1} \\ 0 \\ 0 \end{bmatrix} Q_h + \begin{bmatrix} 0 & 0 & 0 \\ 0 & 0 & 0 \\ \frac{1}{C_3} & \frac{1}{C_3R_r} & \frac{1}{C_3R_c} \end{bmatrix} \begin{bmatrix} I_s \\ T_r \\ T_a \end{bmatrix} \tag{12}$$

where the term $\boldsymbol{W}$ of Eq. (5) has been split into two parts: $\boldsymbol{B}Q_h$, which includes the control variable Q_h, and **EU**, where the uncontrollable environmental variables were collected in $\boldsymbol{U}$. As an example, the state equation for T_1 becomes:

$$\dot{T}_1=\frac{Q_h-Q_{12}}{C_1}=\frac{Q_h-(T_1-T_2)/R_{12}}{C_1}=\frac{-1}{C_1R_{12}}\bullet T_1+\frac{1}{C_1R_{12}}\bullet T_2+\frac{1}{C_1}\bullet Q_h \tag{13}$$

3. Model validation

The requirement for the CHTC sensor model was that it should

allow prediction of the (largest) sensor time constant. To provide evidence that this requirement was fulfilled, we performed a series of step response experiments for various sensor configurations.

3.1. Step response modelling

In a step response experiment, the system is first brought to the initial state $\boldsymbol{T}(t_0)$, at time t_0, by applying the input signal $Q_h \neq 0$ (or by other means), and then, in the second stage, is allowed to relax until a steady reference state $\boldsymbol{T_{ref}}$ is reached. With the step temperature $\Delta\boldsymbol{T}=\boldsymbol{T}-\boldsymbol{T_{ref}}$ inserted into Eq. (12), we obtain:

$$\Delta\dot{\boldsymbol{T}}=\boldsymbol{A}\Delta\boldsymbol{T} \tag{14}$$

$$\boldsymbol{T_{ref}}=-\boldsymbol{A}^{-1}\left(\boldsymbol{B}Q_h+\boldsymbol{EU}\right) \tag{15}$$

Eigenvalue decomposition of $\boldsymbol{A}$ yields $\boldsymbol{A}=\boldsymbol{VDV}^{-1}$, where $\boldsymbol{D}=\begin{bmatrix} s_1 & 0 & 0 \\ 0 & s_2 & 0 \\ 0 & 0 & s_3 \end{bmatrix}$ is the diagonal matrix of eigenvalues s_i to matrix $\boldsymbol{A}$, and the corresponding eigenvectors $\boldsymbol{\nu_i}$ form the columns of matrix $\boldsymbol{V}=[\boldsymbol{\nu}_1, \boldsymbol{\nu}_2, \boldsymbol{\nu}_3]$. The present system has three time constants $\tau_i=1/|s_i|$, one for each eigenvalue s_i. With the substitution $\Delta\boldsymbol{T}=\boldsymbol{VZ}$ in Eq. (14), we obtain:

$$\dot{\boldsymbol{Z}}=\boldsymbol{DZ} \tag{16}$$

The step response of the system is then given as (cf. ref. [15]):

$$\Delta\boldsymbol{T}(t)=\exp\left[\boldsymbol{A}(t-t_0)\right]\Delta\boldsymbol{T}(t_0)=$$
$$=Z_1(t_0)\exp\left[s_1(t-t_0)\right]\boldsymbol{\nu}_1+Z_2(t_0)\exp\left[s_2(t-t_0)\right]\boldsymbol{\nu}_2+Z_3(t_0)$$
$$\exp\left[s_3(t-t_0)\right]\boldsymbol{\nu}_3, \tag{17}$$

where the initial state values are given by

$$\begin{bmatrix} Z_1(t_0) \\ Z_2(t_0) \\ Z_3(t_0) \end{bmatrix}=\boldsymbol{V}^{-1}\Delta\boldsymbol{T}(t_0) \tag{18}$$

We directly use the heat balance for the top sensor surface, $Q_s=-I_s+Q_r+Q_c$, to derive the expression for the surface reference temperature, $T_{3,\,ref}$. With $Q_s=Q_h=0$, and model expressions for Q_r and Q_c inserted, we have:

$$T_{3,ref}=\frac{I_s+\frac{T_r}{R_r}+\frac{T_a}{R_c}}{\frac{1}{R_r}+\frac{1}{R_c}} \tag{19}$$

In the present case (see below), where $I_s = 0$, and $T_r = T_a$, we obtained $T_{3,ref}=T_a$. Note that $T_{3,ref}$ is by definition the sol-air temperature [16,17], which is the temperature of the surface of an adiabatic wall, exposed to solar irradiance, thermal radiative exchange and convective heat transfer.

3.2. Step response experiments

The main purpose of the step response experiments was to estimate the largest of the sensor time constants, i.e. $\tau_{max}=1/|s_{min}|$. For this purpose, the experiments were performed in a stable laboratory environment, where T_a stays constant, T_r could be assumed to equal T_a (sensor top surface exposed only to surfaces that are approximately at laboratory air temperature), and $I_s = 0$ (no daylight or artificial light). In the experiments, the h_c at the sensor front surface was kept constant by forcing a steady flow of air over this surface. In the series of step response experiments, the average h_c value was 40.9 (SD = 0.9) W m^{-2} K^{-1}.

Fig. 1 shows a schematic drawing of the CHTC sensor construction. The heat flux Q_h was supplied by applying a 25.0 V DC voltage across a resistive (633 Ω) heater foil (polyimide thermofoil, Minco, USA), positioned between two copper plates, which together forms the bottom sensor layer. The temperature T_3 (and T_1 in one case) was measured using a platinum resistance thermometer (PRT; class A, 100 Ω, 4-wire, 4 mm diameter probe, Jumo, Fulda, Germany), whose time constant was estimated to equal 2.0 min. A ventilated and shielded PRT (class DIN B/3, 100 Ω, 4-wire, model 41342, with model 43502 shield, Young, USA) was used for measurement of T_a. The Hukseflux HFM (see specification above) consists of a series of thermocouples, arranged so as to measure the temperature difference T_{diff} across the HFM plate, which is calibrated to measure the heat flux q_{HFM} (W m^{-2}) through the HFM. However, the manufacturer´s calibration certificate provides only the value of the constant k (μV/(W m^{-2})), which relates q_{HFM} to E (μV), the voltage output signal from the HFM. Thermal contact between sensor components was ensured by applying a thin layer of silicon heat-sink paste to the contacting surfaces. The sensor was insulated, using extruded polystyrene material (Sundolit XPS300BE, Sunde Group, Oslo, Norway; λ_{ins} = ca 0.035 W m^{-1} K^{-1}), with layer thickness equal to a minimum of about 60 mm, at both side and bottom surfaces. The sensor top surface was coated with 0.10 mm black matt paint coating (Nextel-Velvet-coating 811-21; Mankiewicz Gebr., Hamburg, Germany), with an emissivity ε_s measured to the value 0.943 [18]. Measurement input signals, from thermometers and the HFM, and digital on/off switching of the heater voltage or fan, were collected or sent simultaneously at a 0.02 Hz frequency, using the data acquisition system (NI cDAQ-9178, modules NI9217 (for PRTs), NI9219 (for HFM), and NI9401 (digital output); National instruments, Austin, USA), which was run under the Labview software. The forced air flow, applied to the sensor surface, was generated by a 119 × 119 mm, DC axial fan (EBM-Papst, Mulfingen, Germany), positioned 0.29 m from the edge of the sensor top surface. The wind speed above the surface was about 2.5 ms^{-1}, and turbulent conditions probably existed. For model matrix calculations, the MATLAB software (R2015b, MatchWorks Inc., Natick, USA) was used.

The top surface temperature $T_s(t)$ was monitored in the step response experiments. The step was applied in two different ways: (i) The heater heat flux Q_h was supplied at a constant rate, with a step-down to zero at time t_0, or (ii), with Q_h held constant throughout the experiment, the fan was turned on at time t_0, thereby producing a step in h_c from free to forced convection conditions. For $t > t_0$, both these kinds of steps yield a step-down in T_s, while h_c is at a constant and equal level. The difference is that the sensor was excited to different initial temperature states. The steady-state initial values, $T_s(t_0)$, $T_a(t_0)$, and $q_{HFM}(t_0)$, were obtained as the average values of the 100 samples taken immediately prior to time t_0. Data (n = 100) for estimation of T_{ref} were sampled at $t >> t_0$, where the final steady-state had been reached. For evaluation of the time constant, the step temperature $\Delta T_s(t)=T_s(t)-T_{ref}$ was first calculated, and then the natural logarithm of $\Delta T_s(t)$ was plotted against time t, including only those data points where $\Delta T_s(t)>0.05\bullet\Delta T_s(t_0)$, and $t \geq t_0$. Finally, ordinary linear regression gives the slope b, and the experimentally estimated time constant $\tau_{exp}=-1/|b|$.

In order to obtain a range of system time constants for comparison between experimental and model results, we performed the step response experiments using three different sensor configurations (L, M, and S). These differed only in the thickness and thermal capacitance of the bottom layer (see Table 2).

Table 2
Configurations of h_c sensors.

h_c Sensor	H_1	H_2 (HFM)	H_3	C_1	R^*	C_2	C_3
	(m)	(m)	(m)				
L	0.0240	0.005	0.012	415	0.625	144	207
M	0.0135	"	"	233	"	"	"
S	0.0030	"	"	51.9	"	"	"

Total h_c sensor height $H = H_1+H_2+H_3$, and its circular cross-section has the radius $r = 40$ mm.

* $R = R_{12} = R_{23}$.

4. Results and discussion

The sensor model was validated by comparisons to experimental results using the following indicators: (i) the (largest) system time constant, (ii) the surface temperature time evolution, and (iii) to what extent the supplied electrical power equals the heat flux measured by the HFM. The latter indicator was used to test the model assumption that the sensor insulation layer is an adiabatic wall.

4.1. Time constant

The experimentally estimated and the corresponding modelled time constants, τ_{exp} and τ_{mod} (largest model time constant), respectively, were compared in Fig. 2. The agreement between model and experimental results was acceptable for the purpose of the present work. The observed deviation could to some extent be explained by heat loss through the insulation, or through the PRT leads, since this will decrease τ_{exp}. As an alternative, bias in model parameter estimates could also explain part of the discrepancy between τ_{exp} and τ_{mod}. Note that the model parameters, i.e. the R and C elements, except R_c and R_r, were estimated based solely on material data available prior to any model predictions were performed. For this reason, and especially for C_2 (HFM capacitance), there is probably a significant bias in the parameter estimates. In fact, when C_2 was decreased by 40%, then the model time constant τ_{mod} decreased by 4.6 min, the same amount for all sensors L, M, and S. The HFM specification states that the HFM´s response time should equal "average soil". Therefore, with C_2 material property values instead selected as $\rho = 2050\ \mathrm{kg\,m^{-3}}$ and $c_v = 1840\ \mathrm{J\,kg^{-1}\,K^{-1}}$, corresponding to data for "soil" in Table A3 in ref. [13], we obtain a 34% reduction in the C_2 estimate in comparison to the presently used value.

4.2. Temperature evolution

The time evolution of the surface temperature T_3 was modelled with input data from the Q_h and h_c step experiments on sensor L. In this experiment, $T_3(t_0)$ was measured directly, while $T_1(t_0)$ was estimated as

$$T_1(t_0)=T_3(t_0)+a_1 \bullet q_{HFM}(t_0) \tag{20}$$

where a_1 is a calibration constant relating the heat flux as measured by the HFM, $q_{\mathrm{HFM}}(t)$, to the temperature difference across the HFM, $T_{diff}=T_1(t)-T_3(t)$. The constant a_1 was estimated in a separate experiment, where also T_1 was measured using a PRT probe. The HFM initial temperature was estimated as $T_2(t_0)=\big(T_1(t_0)+T_3(t_0)\big)/2$, assuming a linear temperature fall across the HFM layer.

For sensor L we thus have the model matrices:

$$\boldsymbol{A}=\begin{bmatrix} -0.00386 & 0.00386 & 0 \\ 0.0111 & -0.0222 & 0.0111 \\ 0 & 0.00771 & -0.00882 \end{bmatrix},\ \boldsymbol{B}=\begin{bmatrix} 0.00241 \\ 0 \\ 0 \end{bmatrix},\ \text{and}$$

$$\boldsymbol{E}=\begin{bmatrix} 0 & 0 & 0 \\ 0 & 0 & 0 \\ 0.00482 & 0.000134 & 0.000974 \end{bmatrix},$$

$$\text{with } \boldsymbol{D}=\begin{bmatrix} -0.0284 & 0 & 0 \\ 0 & -0.000267 & 0 \\ 0 & 0 & -0.00627 \end{bmatrix},\ \text{and}$$

$$\boldsymbol{V}=\begin{bmatrix} 0.1449 & 0.6237 & -0.4471 \\ -0.9203 & 0.5805 & 0.2803 \\ 0.3633 & 0.5235 & 0.8494 \end{bmatrix} \tag{21}$$

From matrix D, we see that $s_2 = -0.000267\ \mathrm{s^{-1}}$ yields the model prediction of the largest time constant $\tau_{mod}=1/|s_2|=62.5$ min. We also note that the next largest system time constant was $\tau_3=1/|s_3|=2.66$ min. With $\boldsymbol{T}(t_o)$ estimated as above, we subtract T_{ref} to obtain $\Delta\boldsymbol{T}(t_o)$, which inserted into Eq. (18) yields

$$\begin{bmatrix} Z_1(t_0) \\ Z_2(t_0) \\ Z_3(t_0) \end{bmatrix}=\boldsymbol{V}^{-1}\Delta\boldsymbol{T}(t_0)=\begin{bmatrix} 0.0254 \\ 8.7371 \\ -0.3914 \end{bmatrix} \tag{22}$$

Finally, Eq. (17) gives the time evolution of the sensor surface temperature ΔT_3 for the Q_h-step response experiment as shown in Fig. 3.

4.3. Sensitivity analysis

The sensor system includes the radiative and the convective surface resistances, R_r and R_c, respectively, and changes in these will have effect on the system time constant. For a high emissivity sensor surface, R_r changes with about 1% per Kelvin change in T_{sr} (cf. Eq. (10)), with an approximate R_r value equal to $35\ \mathrm{KW^{-1}}$ at 293 K. Changes in R_c $(=1/ah_c)$ are induced by changes in air flow conditions, which may increase h_c from ca $6\ \mathrm{W\,m^{-2}\,K^{-1}}$ at free convection, up to values in the range 40–66 $\mathrm{Wm^{-2}\,K^{-1}}$, using Jürges´ empirical h_c-V-correlation [1] for wind speeds ranging between 9 and $18\ \mathrm{ms^{-1}}$. With the present sensor, the corresponding R_c values are ca 33, 5.0, and $3.0\ \mathrm{KW^{-1}}$, for the h_c values 6, 40, and $66\ \mathrm{W\,m^{-2}\,K^{-1}}$, respectively (Fig. 4).

Table 3 shows the results of a sensitivity analysis of the predicted time constant τ, using the model above. Clearly, under free convection, we have the largest time constants, while at windy

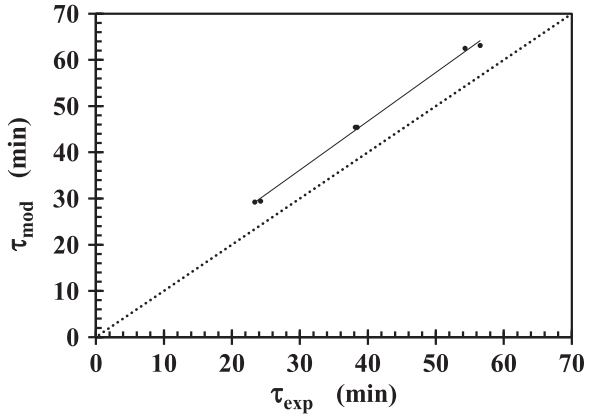

Fig. 3. Comparison of time constants between experiment (τ_{exp}) and model (τ_{mod}). The sensors L, M, and S, were each used in two differently excited step response experiments (step in Q_h or h_c). The regression equation (solid line) is: $y = 4.5(SE = 1.0)+1.055(SE = 0.025)\bullet x$, where SE = standard errors of parameters. Average h_c value = 40.9 (SE = 0.9) $\mathrm{W\,m^{-2}\,K^{-1}}$.

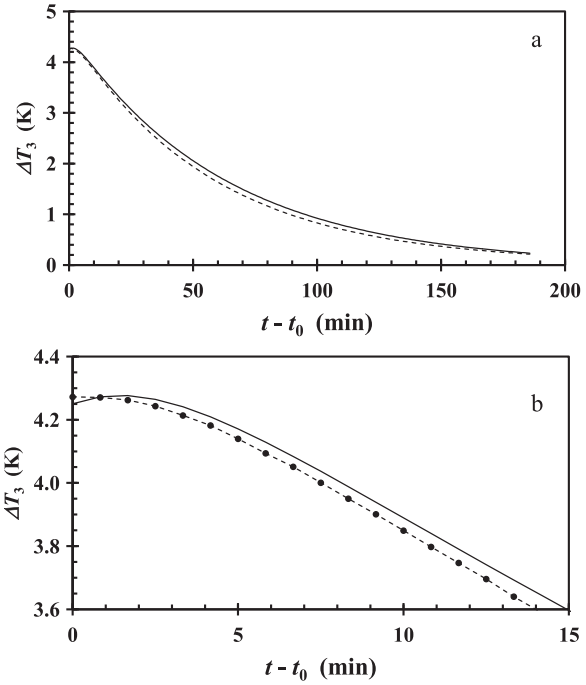

Fig. 4. Time evolution of the ΔT_3 temperature in the L sensor Q_h-step response experiment. Experimental results (filled circles; dashed line) and model predictions (solid line) are shown on two different time scales (a and b). The $h_c = 40.2$ W m^{-2} K^{-1}.

Table 3
Sensitivity analysis of modelled time constant τ.

Sensor L			Sensor S		
R_c (KW^{-1})	R_r (KW^{-1})	τ (min)	R_c (KW^{-1})	R_r (KW^{-1})	τ (min)
33	41	241	33	41	124
33	33	219	33	33	113
5.0	37	63	5.0	37	31
3.0	41	42.9	3.0	41	20.0
3.0	33	42.4	3.0	33	19.7

For estimation of R_c and R_r, $a = 0.005$ m^2, and $\varepsilon_s = 0.943$. The T_{sr} equaled the values 283, 293, and 303 K, for R_r equal to 41, 37, and 33, respectively.

conditions, the time constant could be reduced fivefold. We see from Table 3 that the radiative resistance R_r seems to have only a minor influence on the time constant, even when R_r is in the same magnitude as R_c. A reduction of the surface emissivity will increase R_r, which will further reduce the effect of R_r upon the time constant.

4.4. Heat loss through insulation

The electrically supplied power ($U_e = 25.0$ V, $R_e = 633\ \Omega$) per unit of sensor top surface, $q_e = U_e^2/(aR_e)$ (W m^{-2}), at steady-state, was compared to the heat fluxes measured by the HFM, q_{HFM}. For the six step response experiments, performed at mean $h_c = 40.9$ W m^{-2} K^{-1} (cf. Fig. 3), the average q_{HFM}/q_e=0.999 (SD = 0.016). This indicates that heat loss through the insulation is negligible under forced convection.

Under free convection, the time constant for sensor S was experimentally estimated in a Q_h-step response experiment to be $\tau_{exp} = 116.7$ min, while the model prediction was $\tau_{mod} = 103.3$ min ($h_c = 7.33$, $R_c = 27.2$ KW^{-1}, $T_{sr} = 299.6$ K, and $R_r = 34.6$ KW^{-1}). The agreement in time constant estimates indicates that model performance is acceptable also under free convection conditions. However, this experiment showed the presence of heat loss Q_{ins} through the insulation layer, since only 91.0% of the electrically supplied power was recovered as heat flux through the HFM. This yields the estimate $Q_{ins} = 0.081$ W.

The presence of heat leakage through the insulation surrounding the bottom part of the sensor implies that there is also a similar heat loss for the upper part of the sensor. It was previously pointed out that such heat loss through the insulation above the HFM will cause a systematic error in the measurement of h_c [19], and must therefore be minimized. Note that this error due to heat loss through the insulation occurs under free convection conditions where h_c is at a low value. Under such conditions, convective heat transfer is restricted by an increased R_c resistance, and some heat is instead conducted through the insulation.

4.5. Measurement accuracy

The principle assumption for this measurement method is that the sensor system is in a steady-state, and this requires that the system time constants are smaller than the time-scale of variation in the environmental variables. Typically, the solar irradiance, air temperature, thermal radiation and wind vary on the scale of hours to days, but faster frequencies occur. Assuming that the maximum frequency in these environmental variables is f_{max}, then the Nyquist-Shannon sampling theorem states that a sampling frequency $f_s = 2f_{max}$ is sufficient to enable accurate reconstruction of the sampled signal [20]. In order for the sensor to reach the steady-state, within the sampling time interval $\Delta t = 1/f_s = 1/(2f_{max})$, and within 1% accuracy, its time constant should be $\tau < \Delta t/5 = 1/(10f_{max})$ (cf. [21]).

The measurement uncertainty is estimated after corrections for systematic errors, and include the uncertainty of such corrections and estimates of random measurement errors (cf. [19]). In the case where significant heat loss through the insulation layer is present, and could not be further reduced by improved insulation, the heat flux measurement result (q_{HFM}) must be corrected, and the correction uncertainty be estimated. The present sensor model could be used for evaluation of two types of errors where the system dynamics is involved: (i) the settling error, and (ii) the lag error [21]. The settling response error occurs when the sensor, exposed to a constant h_c-value, is not allowed sufficient time to reach the steady-state, after turning on the sensor. To ensure a settling error $< 1\%$, a waiting time of at least five time constants is required [21]. With a steadily changing h_c-value, there is a lag error, due to the fact that the sensor response lags behind the change in h_c. The lag error $\Delta h_{c,lag}$ is estimated as:

$$\Delta h_{c,lag} = -\tau \bullet dh_c/dt \tag{23}$$

where dh_c/dt is the rate of change in h_c (cf. [21]). For example, with $\tau = 1$ h, and $dh_c/dt = 1$ W m^{-2} K^{-1} h^{-1} (corresponding to 0.25 ms^{-1} change in wind speed per hour, using Jürges' model), we obtain the lag error $\Delta h_{c,lag} = -1$ W m^{-2} K^{-1}.

The present sensor model was applied to estimate the time constant of the heated gradient sensor most commonly used in building science. This sensor was designed by Ito et al. [2], and subsequently used by others [3–6], with slight modifications. The bottom layer of the Ito design consisted of 1 mm Aluminum, and 2 mm Copper, with a thin heater in between. The HFM was 3 mm thick, made of neoprene (soft rubber), and the top layer was Copper, with 1 mm thickness. With thermal properties obtained from [13], we estimated the model sensor parameters as follows: $C_1 = 46.8$ J K^{-1}, $C_2 = 33.2$ J K^{-1}, $R = 4.62$ KW^{-1}, and $C_3 = 17.3$ J K^{-1}. With $T_{sr} = 293$ K, the model predictions of the time constant τ were 32, 11, and 8.4 min, for $h_c = 6$, 40 and 66 W m^{-2} K^{-1}, respectively. The top surface was painted black, and therefore its emissivity should have been around 0.95. The sensor was backed

by a 140 mm thick insulation layer, and although its thermal conductivity was unknown, the adiabatic wall requirement was probably fulfilled. For this reason, there should have been only negligible heat losses through the insulation layer, and therefore insignificant systematic error in the measurement of q_d, the conductive heat flux reaching the sensor surface. Measured data were sampled at the frequency 1 min^{-1}, and averaged over a 15 min time period [2], which suffice for accurate sampling of the sensor signal, even when operated under fast response conditions (high h_c). Since the rate of change in h_c (related to wind speed) during their measurements was not reported, it was not possible to estimate dynamic errors in their results.

4.6. System control

In some applications of this type of sensor, a control system has been used. For examples, the temperature difference between the sensor surface and the air, was controlled by varying the supplied electrical power [5,6]. In another case, where the Ito two-sensor method was applied, the controlled quantity was the temperature difference between the two sensor surfaces [3]. In none of these cases, there was any discussion on how the presence of a control system effects system performance, e.g. in terms of system time constants, or measurement uncertainty. The present sensor model is formulated as a linear system of equations, with state-space variables. This type of model formulation enables the application of linear control theory, and thereby the future investigation of system performance, for cases where the sensor is operated with a control system.

4.7. System design and operating conditions

Decrease of the system time constant leads to reduction in dynamic errors, which means that higher frequency variations in h_c could be measured, without violation of the method requirement to measure under steady-state conditions. With our sensor design, the lower limit for the system time constant is set by the HFM and the PRT sensors used, which have time constants equal to 3 and 2 min, respectively (the latter was experimentally estimated). The time constant for temperature measurement could be reduced down to the seconds-level by replacing the PRT with, for examples, thermocouples or a thermal camera. However, the temperature accuracy may suffer by such actions. The contribution of the HFM to the system time constant could be eliminated by simply removing the HFM from the design, and instead measure the conductive heat flux as the electrically supplied power. This requires, of course, that heat loss through the insulation layer is negligible for all operating conditions. We have seen that heat loss may occur when the sensor is operated under free convection conditions.

As shown above, for a given sensor time constant τ (depends on h_c), it is required that the sampling frequency is selected to be $f_s \leq 1/(5\tau)$, in order to fully utilize the sensors capacity to accurately measure the varying h_c quantity. The first measurement should be acquired after a waiting time of at least five time constants, in order to reduce the settling error. If there is a constant rate of change in the h_c-value in a series of measurements, then this rate of change should be estimated, and used for correction of the lag error.

Acknowledgements

Financial support for this work was gratefully received from the Swedish Energy Agency, through IQ Samhällsbyggnad and the E2B2 program (project no. 39699-1), and from the Kempe Foundations. We also want to thank Fredrik Holmgren and Johan Haake for skillful technical support in construction of the experimental equipment.

References

[1] W. Jürges, Der wärmeübergang an einer ebenen wand (heat transfer at a plane wall), Gesundh.-Ing. Beih. Nr. 19 (1924).
[2] N. Ito, K. Kimura, J. Oka, A field experiment study on the convective heat transfer coefficient on exterior surface of a building, ASHRAE Trans. 78 (1972) 184–191.
[3] S. Sharples, Full-scale measurements of convective energy losses from exterior building surfaces, Build. Environ. 19 (1984) 31–39.
[4] D.L. Loveday, A.H. Taki, Convective heat transfer coefficients at a plane surface on a full-scale building facade, Int. J. Heat. Mass. Transf. 39 (1996) 1729–1742.
[5] S.E.G. Jayamaha, N.E. Wijeysundera, S.K. Chou, Measurement of the heat transfer coefficient of walls, Build. Environ. 31 (1996) 399–407.
[6] Y. Liu, D.J. Harris, Full-scale measurements of convective coefficient on external surface of a low-rise building in sheltered conditions, Build. Environ. 42 (2007) 2718–2736.
[7] M. Mirsadeghi, D. Cóstola, B. Blocken, J.L.M. Hensen, Review of external convective heat transfer coefficient models in building energy simulation programs: implementation and uncertainty, Appl. Therm. Eng. 56 (2013) 134–151.
[8] J.A. Palyvos, A survey of wind convection coefficient correlations for building envelope energy systems' modeling, Appl. Therm. Eng. 28 (2008) 801–808.
[9] G.M. Carlomagno, L. de Luca, G. Cardone, T. Astarita, Heat flux sensors for infrared thermography in convective heat transfer, Sensors 14 (2014) 21065–21116.
[10] P.R.N. Childs, J.R. Greenwood, C.A. Long, Heat flux measurement techniques, Proc. Inst. Mech. Eng.: Part C.: J. Mech. Eng. Sci. 213 (1999) 655–677.
[11] J. Taler, D. Taler, Chap. 1: Measurement of heat flux and heat transfer coefficient, in: Heat Flux: Processes, measurement techniques and applications, Nova Sci. Publish. New York, 2012.
[12] D.C. Karnopp, D.L. Margolis, R.C. Rosenberg, System Dynamics. Modeling, Simulation, and Control of Mechatronic Systems, Wiley, 2012.
[13] F.P. Incropera, D.P. DeWitt, Fundamentals of Heat and Mass Transfer, Wiley, 2002.
[14] C.-E. Hagentoft, Introduction to Building Physics, Studentlitteratur, Lund, Sweden, 2001.
[15] H. Madsen, J. Holst, Estimation of continuous-time models for the heat dynamics of a building, Energy Build. 22 (1995) 67–79.
[16] C.O. Mackey, L.T. Wright, The sol-air thermometer - a new instrument, Trans. Am. Soc. Heat. Vent. Eng. 52 (1946) 271–282.
[17] J.F. Kreider, A. Rabl, Heating and cooling of buildings design for efficiency, Mcgraw-Hill, 1994.
[18] J. Lohrengel, R. Todtenhaupt, Wärmeleitfähigkeit, gesamtemissionsgrade und spektrale emissionsgrade der beschichtung Nextel-Velvet-Coating, 811-21 (RAL 900 15 tiefschwarz matt), PTB-Mittelungen, 106, 1996, pp. 259–265.
[19] K.E.A. Ohlsson, R. Östin, T. Olofsson, Accurate and robust measurement of the external convective heat transfer coefficient based on error analysis, Energy Build. 117 (2016) 83–90.
[20] C.E. Shannon, Communication in the presence of noise, Proc. IRE 37 (1949) 10–21.
[21] J.V. Nicholas, D.R. White, Traceable temperatures ISBN 0 471 49291 4, 2nd ed., Wiley, 2001.